IEEE Access
Multidisciplinary | Rapid Review | Open Access Journal

Received 26 April 2023, accepted 11 May 2023, date of publication 15 May 2023, date of current version 24 May 2023.

Digital Object Identifier 10.1109/ACCESS.2023.3276649

RESEARCH ARTICLE

Design and Implementation of a Soft-Switching Converter With High Step-Up Ratio

KUEI-HSIANG CHAO, (Member, IEEE), YING-PIAO KUO, AND HONG-HAN CHEN
Department of Electrical Engineering, National Chin-Yi University of Technology, Taiping, Taichung 411030, Taiwan

Corresponding author: Kuei-Hsiang Chao (chaokh@ncut.edu.tw)

This work was supported by the Ministry of Science and Technology, Taiwan, under Grant MOST 110-2221-E-167-007-MY2.

ABSTRACT The main purpose of this paper is the development of a DC/DC boost converter with high conversion efficiency. The proposed converter has high step-up ratio and is equipped with soft-switching technology. The main inductor used in the developed converter is the coupled inductor rather than the general inductor, therefore, the voltage conversion ratio of the converter can be improved, so that the high voltage conversion ratio characteristics of the converter power switch can be obtained within the same duty cycle. The developed converter is connected to a resonance branch circuit in the traditional high step-up converter, and is able to achieve zero-voltage switching (ZVS) with the main switch using a simple power switch signal control to reduce the switching loss caused by the traditional hard switching method in the high step-up converter, thereby improving converter efficiency. To verify the performance of the proposed converter, a circuit analysis on the high step-up soft-switching converter is first performed, and proceed to designing each component in the circuit. Then, the feasibility of the proposed converter is verified using the PSIM simulation software. Finally, actualize the proposed high step-up soft-switching boost converter with the TMS320F2809 digital signal processor (DSP), and verify that the main switch can indeed achieve zero-voltage switch, and that the conversion efficiency can reach as high as 91% when the developed converter is under full load of 300W, proof that the developed converter truly has excellent conversion performance.

INDEX TERMS Coupled inductor, high step-up converter, soft-switching converter, zero-voltage switching (ZVS), digital signal processor (DSP).

I. INTRODUCTION

In recent years, renewable energy setups are being actively promoted around the world, among which, the photovoltaic power generation system is currently one of the most technologically mature and cleanest renewable energy resources known because sunlight has the advantage of being inexhaustible. As power electronic technologies become increasingly mature, power electronic converters are now being widely used in photovoltaic power generation systems, which improves the power generation efficiency of these systems. Thus, technologies which use soft-switching to reduce the converter switching loss and increase power conversion efficiency has been gaining increasing attention. For this, this paper will focus on the development of a high-efficiency converter [1], [2] to be used on the photovoltaic power generation system [3], [4].

For traditional hard-switching DC-DC converters [5], [6], the conversion efficiency is low, the voltage step-up ratio is low, and the switching stress of the power switch is large. Although they can be combined with the soft-switching technique [7], [8], [9], [10], [11], [12], [13], [14] so that they have benefits of fewer circuit components, simpler structure, and ease of control while increasing the conversion efficiency, however, since power switch operation is bounded by the normal duty cycle, the voltage conversion ratio is limited. Furthermore, when higher DC voltage output is needed, the switch component needs to work under a greater duty cycle, but the greater duty cycle will cause the current which passes through the power switch to increase, which may lead to burn-out due to overheating if the power switch is operated for extended time under high duty cycle.

The associate editor coordinating the review of this manuscript and approving it for publication was Ton Duc Do.

In recent years, many scholars have proposed the circuit structure of the high step-up converter. Although higher voltage gains can be obtained using the coupled inductor [15], [16], [17], [18], [19] turns ratio, an excessively high couple inductor turns ratio can easily cause problems such as larger current ripples and oversized inductor volumes. If the soft-switching technique is not used on the switch component, it will lead to switching power losses when the switch component is turned-on and turned-off, and these power losses will increase as switching frequency and input voltage increases. Therefore, the switching frequency and power density of the converter is limited and can easily cause the switch component to overheat, leading to problems of reduced lifespan and decreased efficiency.

To resolve the above high step-up converter flaw, this paper has proposed a high step-up soft-switching converter which uses the coupled inductor rather than the general inductor to increase the voltage conversion ratio of the converter. Additionally, the main switch zero-voltage switch (ZVS) can be done through the simple power switch signal control to reduce the electromagnetic interference (EMI) and voltage switching stress, and improve the switching frequency in the converter, thereby reducing the volume and weight of the filter to improve the overall efficiency of the converter. The PSIM simulation software [20] will be used in this paper to build the circuit structure of the proposed converter, and feasibility of the mentioned converter will be verified with through the simulated analysis. Finally, the TMS320F2809 digital signal processor [21] manufactured by Texas Instruments will be used as the control core during implementation to verify that the proposed high step-up soft-switching converter truly has better conversion performance.

II. PROPOSED HIGH STEP-UP CONVERTER

A. CIRCUIT ANALYSIS OF THE HIGH STEP-UP HARD-SWITCHING CONVERTER

Fig. 1 is the circuit structure of the high step-up hard-switching converter, where the energy-storage inductor is replaced with the coupled inductor in the traditional boost converter, so that the voltage conversion ratio of the converter can be increased through the turns ratio of the coupled inductor, and has the advantages of simpler circuit structure and ease of control. The operation of this converter circuit can be divided into two operating modes of power switch conduction and cutoff. When the power switch is conducted, the duty cycle D within a cycle time T of the converter can be represented in (1).

$$D \triangleq \frac{t_{on}}{T} = \frac{t_{on}}{t_{on} + t_{off}} \tag{1}$$

where t_{on} is the power switch conduction time within a cycle, and t_{off} is the cutoff time.

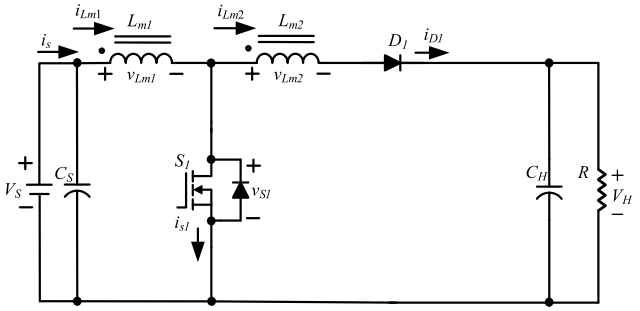

FIGURE 1. Circuit structure of the high step-up hard-switching converter.

1) POWER SWITCH CONDUCTION ($0 \le t_{on} \le DT$)

When the power switch S_1 is conducted, the diode D_1 is cutoff at this time; the equivalent circuit is shown in Fig. 2, and the turns ratio N of the coupled inductor is defined in (2). At this time, the inductor voltage v_{Lm1} and v_{Lm2} are shown in (3) and (4), respectively, and the voltage v_L at the two terminals of the coupled inductor can be represented in (5).

$$N \triangleq \frac{N_2}{N_1} \tag{2}$$

$$v_{Lm1} = V_S \tag{3}$$

$$v_{Lm2} = V_S \frac{N_2}{N_1} = V_S N \tag{4}$$

$$v_L \triangleq v_{Lm1} + v_{Lm2} = (1+N)V_S \tag{5}$$

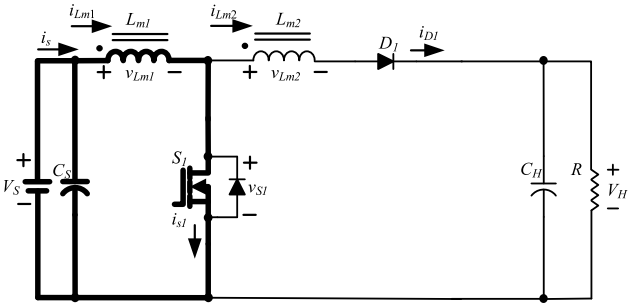

FIGURE 2. Equivalent circuit of the high step-up hard-switching converter with conducted main switch S_1.

2) POWER SWITCH CUTOFF ($DT \le t_{off} \le T$)

When the power switch S_1 is cutoff, the diode D_1 is conducted at this time; the equivalent circuit is shown in Fig. 3, and the voltages v_L at the two terminals of the coupled inductor is shown in (6).

$$v_L = v_{Lm1} + v_{Lm2} = V_S - V_H \tag{6}$$

According to the volt-second balance for the inductor, (7) can be derived from (5) and (6), then the conversion ratio between the output voltage V_H and input voltage V_S shown in (8) can be obtained after rearrangement.

$$(1+N)V_S DT + (V_S - V_H)(1-D)T = 0 \tag{7}$$

$$\frac{V_H}{V_S} = \frac{(1+ND)}{(1-D)} \tag{8}$$

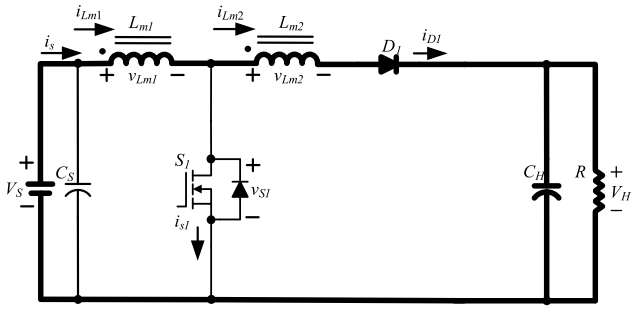

FIGURE 3. Equivalent circuit of the high step-up hard-switching converter with cutoff main switch S_1.

From (8), the relationship between voltage gain and duty cycle of the converter is represented in Fig. 4. It can be observed from Fig. 4, under the same duty cycle, the conversion ratio of the converter can be increased through the turns ratio of the couple inductor.

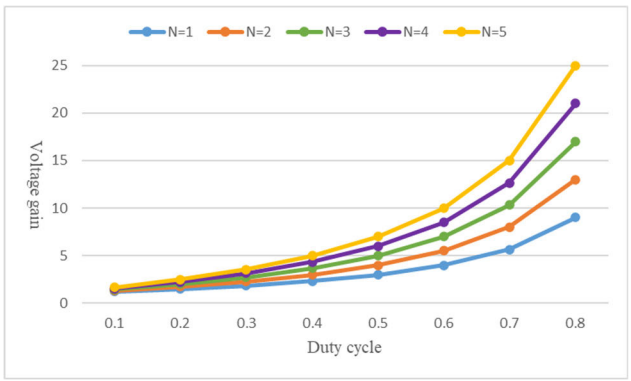

FIGURE 4. Relationship graph between voltage gain and duty cycle of the high step-up hard-switching converter.

B. CIRCUIT ANALYSIS OF THE HIGH STEP-UP SOFT-SWITCHING CONVERTER

Although the coupled inductor can be used to increase voltage conversion ratio of the converter for the high step-up hard-switching converter described in Section A, the voltage or current cannot be brought down to zero before the switch component makes the switch, which leads to switching loss and thereby decreases the overall converter efficiency. Based on this, this paper has proposed a high step-up soft-switching converter with coupled inductor to improve the conversion efficiency; the circuit structure is shown in Fig. 5. The main purpose of the auxiliary switch S_{1r} is to form a resonance trough by allowing the resonance inductor L_r and resonance capacitor C_r to resonate when S_{1r} is turned-on. Fig. 6 is the schematic figure of the proposed converter power switch control signal. Main switch control signal S_1 delayed t_d time before being conducted, and the auxiliary switch S_{1r} is turned on in the delay time t_d to achieve ZVS of the main switch S_1.The characteristic of high step-up ratio of the converter is achieved using the coupled inductor method, and

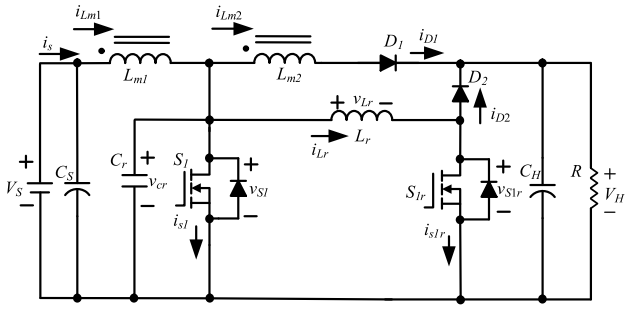

FIGURE 5. Circuit structure of the high step-up soft-switching converter.

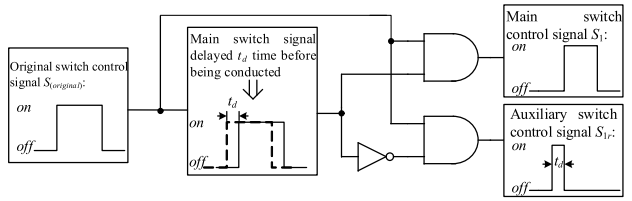

FIGURE 6. Schematic of the switch signal for the proposed high step-up soft-switching converter.

the converter is connected to a resonance branch circuit to achieve the main switch zero-voltage switch function through the power switch signal control. This paper will conduct an analysis on the operating modes for the proposed converter; the whole circuit is divided into seven operating modes, and Fig. 7 is the switching waveforms of each component. Before explaining the operating modes, the following hypothesis must be made:

1) The converter is operating under continuous conduction mode (CCM) and the circuit has reached steady state.

2) All components are ideal components: they are seen as shorted when conducted and open when cutoff, therefore there is no conduction voltage drop on the power switch components.

3) The voltage on the low-voltage side and high-voltage side are maintained at a fixed value.

4) Regard the current of energy-storage inductors L_{m1} and L_{m2} as fixed current sources (that is $i_{Lm1} = I_{Lm1}$, $i_{Lm2} = I_{Lm2}$).

For the proposed high step-up soft-switching boost converter, the power switch operating mode is divided into seven modes between conduction and cutoff, and Fig. 7 is the switching waveforms of the proposed converter for each component under each operating mode.

1) MODE 1 (t_0~t_1)

When operating under Mode 1, the equivalent circuit is shown in Fig. 8; at this time, the main switch S_1 is in cutoff state, the auxiliary switch S_{1r} is conducted first, the voltage of the two terminals of the resonance inductor L_r is V_S; the resonance inductor current i_{Lr} increases at a linear rate from zero, allowing the auxiliary switch to achieve zero-current switching. The circuit equation can be represented in (9),

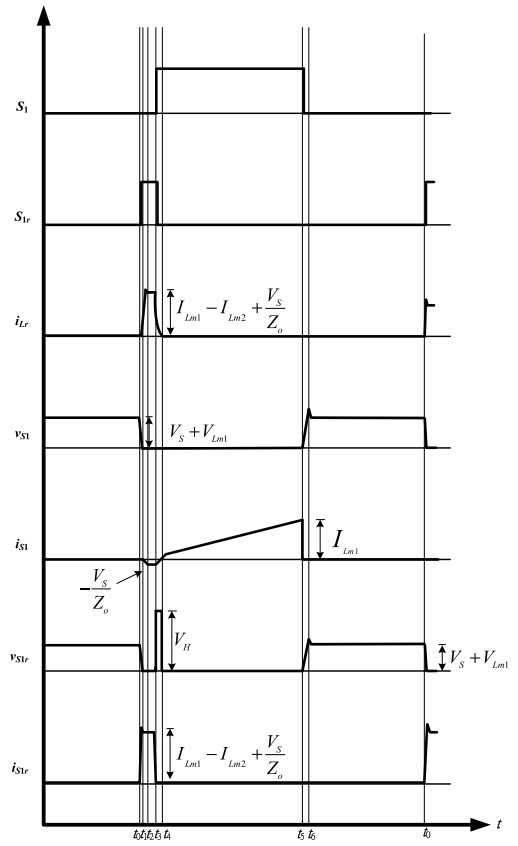

FIGURE 7. Switching waveforms of the proposed converter for each component under each operating mode.

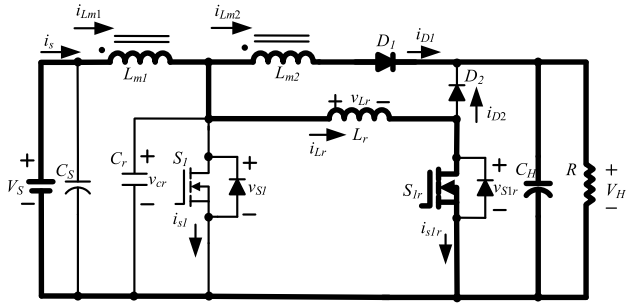

FIGURE 8. Circuit conduction condition for Mode 1.

then i_{Lr} is derived as shown in (10) upon calculations. When the resonance inductor current i_{Lr} increases to $I_{Lm1} - I_{Lm2}$, the diode D_1 from conduction to cutoff achieves zero-voltage switching and the circuit enters operating Mode 2; the operating time of Mode 1 can be obtained as shown in (11) from (10).

$$\begin{cases} L_r \dfrac{di_{Lr}(t)}{dt} = V_S \\ i_{Lr}(t_0) = 0, \end{cases} \qquad t_0 \le t \le t_1 \tag{9}$$

$$i_{Lr}(t) = \frac{V_S}{L_r}(t - t_0) \tag{10}$$

$$T_1 = t_1 - t_0 = \frac{(I_{Lm1} - I_{Lm2})L_r}{V_S} \tag{11}$$

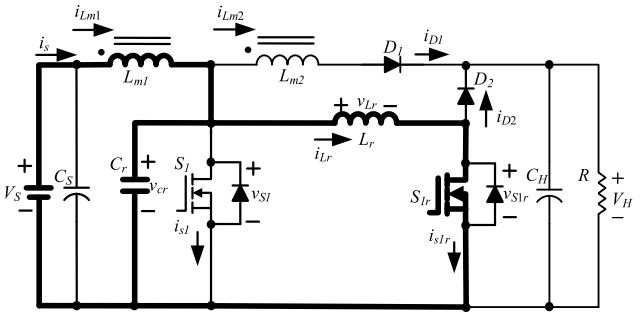

FIGURE 9. Circuit conduction condition for Mode 2.

2) MODE 2 (t_1~t_2)

When entering Mode 2, its equivalent circuit is shown in Fig. 9; at this time, the resonance inductor current i_{Lr} has risen to $I_{Lm1} - I_{Lm2}$ and the auxiliary switch S_{1r} maintains conducted, the resonance inductor current i_{Lr} will continue to increase gradually, and the resonance capacitor C_r begins discharging, thus the resonance inductor L_r and the resonance capacitor C_r form a resonance trough. The circuit equation of this mode is represented in (12), where $v_{Cr}(t)$ and $i_{Lr}(t)$ as in (13) can be solved from (12), and the resonance impedance Z_o and the angular resonance frequency ω_o can be represented in (14). When the resonance capacitor voltage v_{Cr} reduces to zero, at this time $\omega_o(t - t_1) = \frac{\pi}{2}$, therefore, the resonance inductor current i_{Lr} and auxiliary switch current i_{S1r} can be derived from (13) to arrive at (15); the operating time of the operating mode can also be derived as shown in (16) from (13), then the body diode of the main switch S_1 will begin conduction and enter Mode 3.

$$\begin{cases} i_{Lr}(t) + C_r \dfrac{dv_{cr}(t)}{dt} = I_{Lm1} - I_{Lm2} \\ L_r \dfrac{di_{Lr}(t)}{dt} = v_{Cr}(t) \\ v_{Cr}(t_1) = V_S, \end{cases} \qquad t_1 \le t \le t_2 \tag{12}$$

$$\begin{cases} v_{Cr}(t) = V_S \cos\omega_o(t - t_1) \\ i_{Lr}(t) = I_{Lm1} - I_{Lm2} + \dfrac{V_S}{Z_o}\sin\omega_o(t - t_1), \end{cases} \qquad t_1 \le t \le t_2 \tag{13}$$

where

$$\text{Resonance impedance } Z_o \triangleq \sqrt{\frac{L_r}{C_r}}$$

$$\text{resonance frequency } \omega_o \triangleq \frac{1}{\sqrt{L_r C_r}} \tag{14}$$

$$i_{Lr}(t_2) = i_{S1r}(t_2) = I_{Lm1} - I_{Lm2} + \frac{V_S}{Z_o} \tag{15}$$

$$T_2 = t_2 - t_1 = \frac{\pi}{2}\sqrt{L_r C_r} \tag{16}$$

3) MODE 3 (t_2~t_3)

When entering Mode 3, its equivalent circuit is shown in Fig. 10; at this time, the resonance capacitor voltage v_{Cr} has dropped to the minimum negative voltage, causing the body diode of the main switch S_1 to conduct in forward direction so the voltage of the two terminals of the main switch S_1 become zero. The auxiliary switch S_{1r} can be switched from conduction to cutoff at this time, while the main switch S_1 is switched from cutoff to conduction, thus achieving zero-voltage switch for the main switch S_1; the circuit equation can be represented as (17). At this time, the main switch also achieves zero-current switching. In order for the main switch to achieve zero-voltage switching, the time t_d delayed for main switch conduction must satisfy (18), and in order to guarantee the main switch S_1 can still achieve zero-voltage switch during re-load, so, $(\hat{I}_{Lm1} - \hat{I}_{Lm2})_{max}$ is used to find the operating time t_d of the auxiliary switch. Normally, t_d is 5~10% of the switching period, and also considering the cutoff response speed of the auxiliary switch S_{1r}, tolerance time t_ω need to be considered. Therefore, the operating time $t_D = t_d + t_\omega$ of the auxiliary switch can be rewritten as (19).

$$\begin{cases} i_{s1}(t_2) = I_{Lm1} - i_{Lr}(t_2) = I_{Lm2} - \dfrac{V_S}{Z_o} \\ i_{Lr}(t_2) = I_{Lm1} - I_{Lm2} + \dfrac{V_S}{Z_o}, \end{cases} \quad t_2 \le t \le t_3 \tag{17}$$

$$t_d \ge T_1 + T_2 = \frac{(I_{Lm1} - I_{Lm2})L_r}{V_S} + \frac{\pi}{2}\sqrt{L_r C_r} \tag{18}$$

$$t_D \ge t_d + t_\omega = \frac{(\hat{I}_{Lm1} - \hat{I}_{Lm2})_{max} L_r}{V_S} + \frac{\pi}{2}\sqrt{L_r C_r} + t_\omega \tag{19}$$

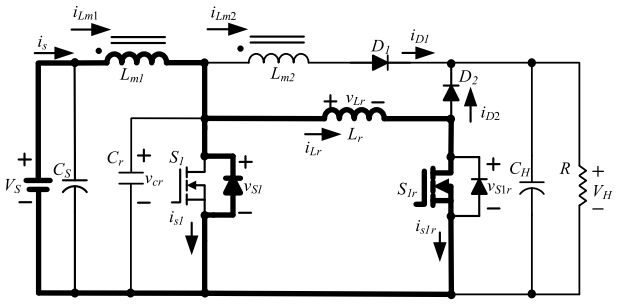

FIGURE 10. Circuit conduction condition for Mode 3.

4) MODE 4 (t_3 ~ t_4)

When entering Mode 4, its equivalent circuit is shown in Fig. 11; at this time, the main switch is conducted S_1, the auxiliary switch S_{1r} enters cutoff from conduction, the diode D_2 is forward conducted, and the resonance inductor transfers the energy to the load. At this time, the resonance inductor voltage is $-V_H$, the auxiliary switch S_{1r} voltage is V_H; the circuit equation of this mode is represented as (20), and solve i_{Lr} to obtain (21). Before finishing this mode, the current i_{S1} of the main switch S_1 will rise to I_{Lm1}, and the resonance inductor current i_{Lr} will drop to zero from $I_{Lm1} - I_{Lm2} + \frac{V_S}{Z_o}$. At this time, the diode D_2 will cutoff with achieving

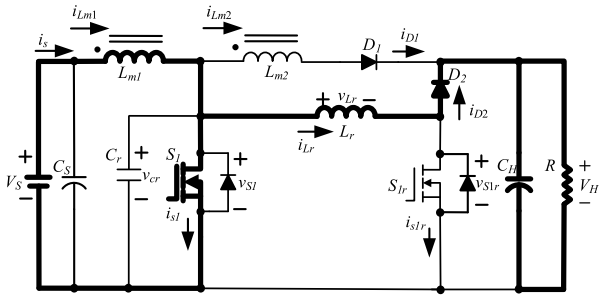

FIGURE 11. Circuit conduction condition for Mode 4.

zero-voltage and zero-current switching. The operating time of (22) under this operating mode can be obtained from (21).

$$\begin{cases} L_r \dfrac{di_{Lr}(t)}{dt} = -V_H \\ i_{Lr}(t_3) = I_{Lm1} - I_{Lm2} + \dfrac{V_S}{Z_o} \\ v_{Cr}(t_3) = 0 \\ i_{s1}(t_3) = I_{Lm1} - i_{Lr}(t_3) \end{cases} \tag{20}$$

$$i_{Lrr}(t) = I_{Lm1} - I_{Lm2} + \frac{V_S}{Z_o} - \frac{V_H}{L_r}(t - t_3), t_3 \le t \le t_4 \tag{21}$$

$$T_4 = t_4 - t_3 = \frac{(I_{Lm1} - I_{Lm2})L_r}{V_H} + \frac{V_S}{V_H}\sqrt{L_r C_r} \tag{22}$$

5) MODE 5 (t_4~t_5)

When entering Mode 5, its equivalent circuit is shown in Fig. 12; at this time, the main switch S_1 continues to be conducted. The circuit equation of this operating mode is represented as (23); (24) can be obtained from (23), and this model needs to consider the impact of the inductor current on the circuit, so the inductor current is not regarded as a constant current source. This mode will continue until the main switch S_1 enters cutoff from conducted, achieving zero-voltage switching.

$$\begin{cases} i_{s1}(t) = I_{Lm1} \\ v_{Cr}(t) = 0, \end{cases} \quad t_4 \le t \le t_5 \tag{23}$$

$$i_{Lm1}(t) = \frac{V_S}{L_{m1}}(t - t_4) \tag{24}$$

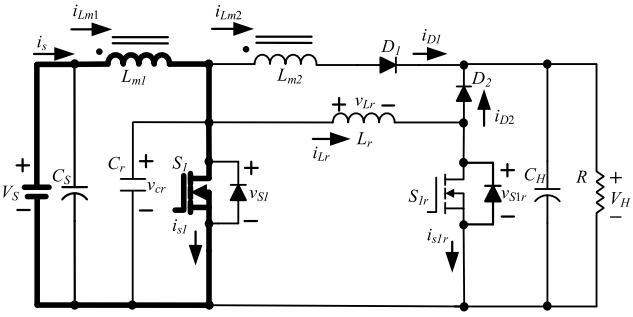

FIGURE 12. Circuit conduction condition for Mode 5.

6) MODE 6 (t_5~t_6)

When entering Mode 6, since the control main switch S_1 is cutoff, its equivalent circuit is shown in Fig. 13, the current I_{Lm1} will charge the resonance capacitor C_r, thus, the resonance capacitor voltage v_{Cr} will increase gradually. The circuit equation of this mode is represented as (25), and v_{Cr} as in (26) can be solved from (25). When the resonance capacitor voltage v_{Cr} is charged to V_S, the operating mode will finish, therefore, the operating time of (27) for this operating mode can be obtained from (26).

$$C_r \frac{dv_{Cr}(t)}{dt} = I_{Lm1} - I_{Lm2}, t_5 \le t \le t_6 \tag{25}$$

$$v_{Cr}(t) = \frac{I_{Lm1} - I_{Lm2}}{C_r}(t - t_5) \tag{26}$$

$$T_6 = t_6 - t_5 = \frac{V_S C_r}{I_{Lm1} - I_{Lm2}} \tag{27}$$

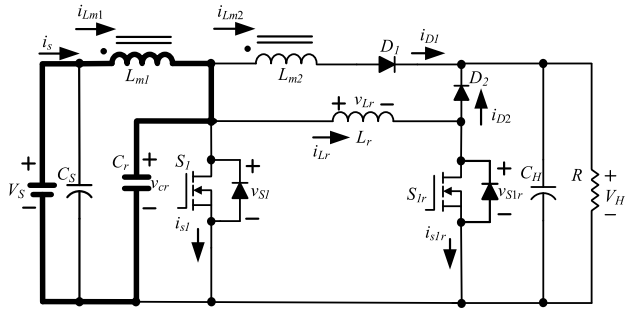

FIGURE 13. Circuit conduction condition for Mode 6.

7) MODE 7 (t_6~t_7)

When entering Mode 7, its equivalent circuit is shown in Fig. 14; at this time, the main switch S_1 continues to be cutoff and the auxiliary switch S_{1r} is also cutoff, thus the coupled inductor will transfer the energy to the load through the diode D_1. The diode D_1 achieves zero-voltage switching. The circuit equation of this operating mode is represented as (28), completing the circuit analysis of the entire switching cycle.

$$\begin{cases} I_{Lm1} = I_{Lm2} \\ v_{Cr}(t) = V_S, \end{cases} \quad t_5 \le t \le t_6 \tag{28}$$

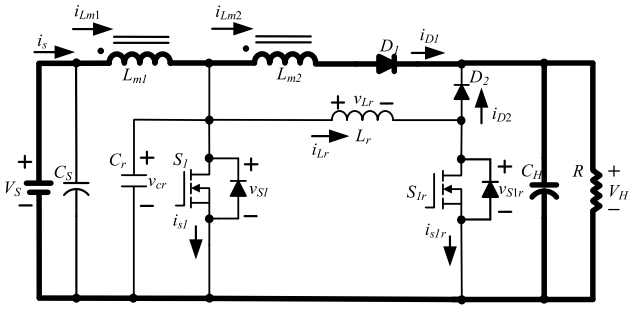

FIGURE 14. Circuit conduction condition for Mode 7.

Based on the operating conditions of each mode, we find out the characteristics of the zero-voltage switching and zero-current switching (ZCS) of each switch component for the proposed high step-up soft-switching converter within a switching cycle, and compile them into Table 1. To demonstrate the performance advantages of the proposed high step-up soft-switching converter, a comparison was made with various high step-up soft-switching converters in terms of voltage gain, rated voltage of MOSFETs, and the numbers of the required MOSFETs, diodes, inductors and capacitors among this proposal and representative pieces of work [8], [9], [10], [11]. The results of their comparison are summarized in Table 2. It can be seen from the Table 2 that the proposed converter can achieve high voltage gain and soft switching with simple signal control and fewer components.

TABLE 1. Sitching characteristics of each component of proposed converter.

Switching characteristics / Switch component	Turned-on	Turned-off
Main switch S_1	ZVS, ZCS	ZVS
Auxiliary switch S_{1r}	ZCS	None
Diode D_1	ZVS	ZVS
Diode D_2	None	ZVS, ZCS

TABLE 2. Performance and requirement comparison among representative types of high step-up soft-switching converters and this proposal.

Converter topology	Converter in [8]	Converter in [9]	Converter in [10]	Converter in [11]	Proposed Converter
Voltage gain	$\frac{2N+2-ND}{1-D}$	$\frac{2+N}{1-D}$	$\frac{2+2N-ND}{1-D}$	$\frac{2+N}{1-D}$	$\frac{1+ND}{1-D}$
Voltage stress on MOSFETs	$\frac{V_O}{2N+2-ND}$	$\frac{V_O}{2+N}$	$\frac{1}{2+2N-ND}$	$\frac{1}{2+N}$	$V_S + V_{Lm1}$
MOSFETs	2	4	2	2	2
Diodes	3	0	3	2	2
Inductors	1	1	1	2	2
Capacitors	4	4	3	4	2
Soft-switching	ZVS	ZVS	ZVS	ZVS	ZVS

III. COMPONENT DESIGN OF PROPOSED CONVERTER

The relevant electrical specifications of the high step-up soft-switching converter proposed in this paper is shown in Table 3. The design of each component value for the converter will be explained in detail below.

TABLE 3. Electrical specifications of proposed converter.

DC input voltage at low-voltage side (V_S)	$V_S = 70V \pm 10\%$
DC output voltage at high-voltage side (V_H)	$V_H = 400V$
Switching Frequency (f)	$f = 25kHz$
Turns ratio of coupled inductor (N)	$N = \frac{N_2}{N_1} = 2$
Coupled inductor (L_{m1})	$L_{m1} = 872\mu H$
Rated output power (P)	$P = 300W$

Assume all components are ideal components, then input power P_{in} should equal to output power P_{out} that is

$$V_S I_{Lm1} = \frac{V_H^2}{R} \tag{29}$$

Replace (8) with (29) to obtain I_{Lm1}, and the result is shown by (30).

$$I_{Lm1} = \frac{V_H^2}{V_S R} = \frac{V_H^2}{V_S^2}\frac{V_S}{R} = \left(\frac{1+ND}{1-D}\right)^2 \frac{V_S}{R} \tag{30}$$

where $\left(\frac{1+ND}{1-D}\right)$ is the voltage conversion ratio of this converter.

When the main switch S_1 is conducted, we can get v_{Lm1}

$$v_{Lm1} = V_S = L_{m1}\frac{di_{Lm1}}{dt} \tag{31}$$

From (31), we find the inductor current is increasing at a linear rate, and in the time $t_{on} = DT$ it is conducted, the amount $\Delta i_{Lm1(closed)}$ of increase of its inductor current is as shown by (32).

$$\Delta i_{L_{m1(closed)}} = \frac{V_S}{L_{m1}} DT \tag{32}$$

Therefore, the maximum and minimum values of the inductor current I_{Lm1} can be shown by (33) and (34), respectively [19].

$$\begin{aligned} I_{Lm1(max)} &= I_{L_{m1}} + \frac{\Delta i_{L_{m1}}}{2} = \left(\frac{1+ND}{1-D}\right)^2 \frac{V_S}{R} + \frac{1}{2}\frac{V_S}{L_{m1}} DT \\ &= V_S\left[\left(\frac{1+ND}{1-D}\right)^2 \frac{1}{R} + \frac{D}{2L_{m1}f}\right] \end{aligned} \tag{33}$$

$$\begin{aligned} I_{Lm1(min)} &= I_{L_{m1}} - \frac{\Delta i_{Lm1}}{2} = \left(\frac{1+ND}{1-D}\right)^2 \frac{V_S}{R} - \frac{1}{2}\frac{V_S}{L_{m1}} DT \\ &= V_S\left[\left(\frac{1+ND}{1-D}\right)^2 \frac{1}{R} - \frac{D}{2L_{m1}f}\right] \end{aligned} \tag{34}$$

For the inductor current to operate in continuous conduction mode (CCM), the minimum value $I_{Lm1(min)}$ of the inductor current must be greater than zero, thus (35) can be obtained from (34).

$$V_S\left[\left(\frac{1+ND}{1-D}\right)^2 \frac{1}{R} - \frac{D}{2L_{m1}f}\right] \geq 0 \tag{35}$$

After rearranging (35), we can obtain the coupled inductor, which by re-testing the smallest value of the inductor value must satisfy (36)

$$L_{m1(min)} \geq \frac{D}{2f}\frac{(1-D)^2 R^2}{(1+ND)} \tag{36}$$

Since the structure of the coupled inductor is similar to an autotransformer type, thus the largest value of I_{Lm2} can be obtained from (37) [19].

$$I_{Lm2(\max)} = \frac{-I_{Lm1(\max)}}{1+N} \tag{37}$$

A. MAIN INDUCTOR COMPONENT DESIGN

In order to allow the converter to operate under continuous conduction mode (CCM) at full load of 300W, the high step-up soft-switching converter proposed in this paper will take on load voltage V_H of 400V; the rated output power of the converter is 300W, thus the rated load resistance is $R = 533.3\Omega$, from the relationship curve of $\frac{D(1-D)^2}{(1+ND)^2}$ against D in Fig. 15, it can be seen that when $D = 0.186$, $\frac{D(1-D)^2}{(1+ND)^2}$ is at its maximum. The duty cycle is substituted (36) by 0.186 to be 698μ H, then, to ensure the converter operates in continuous conduction mode, it needs to be multiplied by the tolerance value of 1.25, therefore, the main inductance L_{m1} selected for this paper is 872μH.

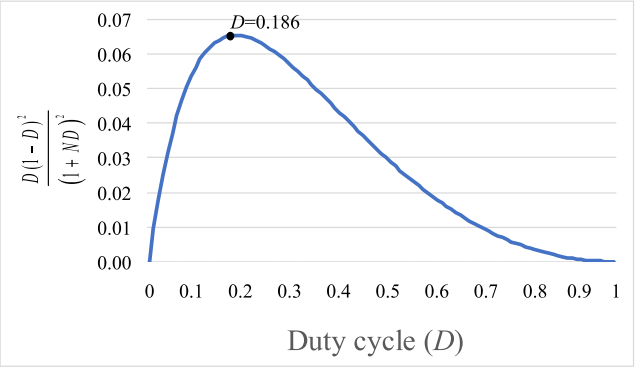

FIGURE 15. Relationship curve of $\frac{D(1-D)^2}{(1+ND)^2}$ against D.

B. RESONANT COMPONENT DESIGN

The resonance capacitor C_r and the resonance inductor L_r can be obtained from (19), and as the selected switch component MOSFET-TK49N65W has a parasitic capacitance of 140 pF in itself, so the resonance capacitor C_r is replaced by the parasitic capacitor. Since the conduction time of the auxiliary

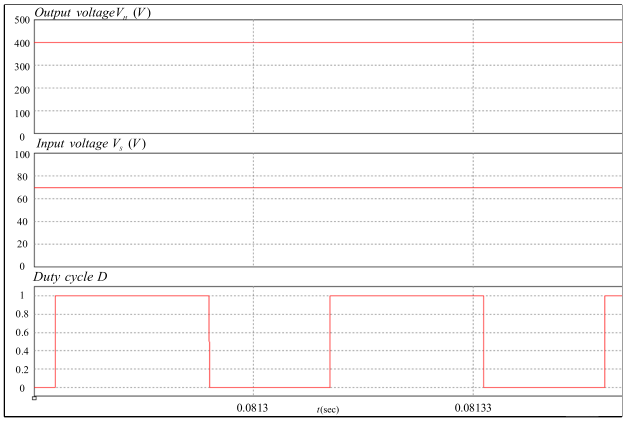

FIGURE 16. Simulation results of the output voltage, input voltage, and duty cycle with the converter working at full load of P_L = 300 W.

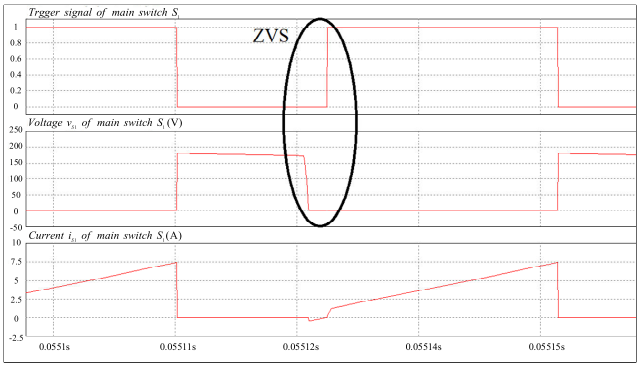

FIGURE 17. Simulated waveforms of each electrical parameter of the converter main switch S_1 at load P_L = 100W.

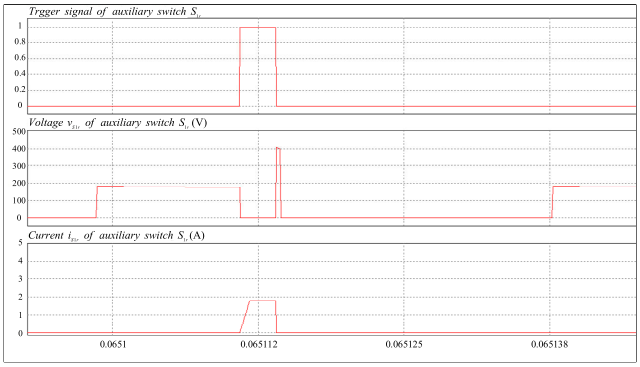

FIGURE 18. Simulated waveforms of each electrical parameter of the converter auxiliary switch S_{1r} at load P_L = 100W.

switch is normally designed to be 5 ∼ 10% of the switching period, so make $t_d = 0.1\text{T} = 4\mu s$ and $t_\omega = 0.01\text{T} = 0.4\mu s$, then obtain the resonance inductor of 27μ H from (19), thus this paper selected 20μH.

IV. SIMULATION RESULTS

After going through the analysis of the circuit structures and detailed explanations of each component design, this paper adopted the PSIM simulation software developed by Powersim Inc. Co. to undergo a simulation of the high step-up

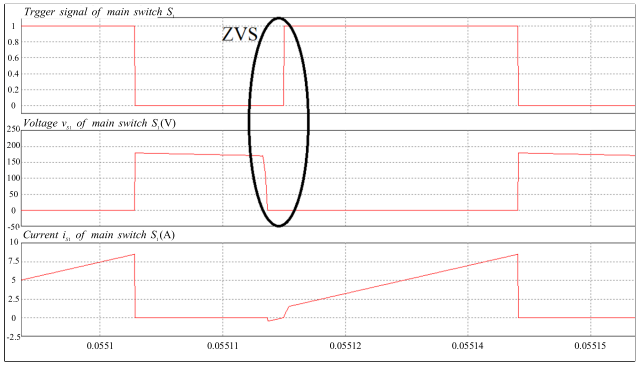

FIGURE 19. Simulated waveforms of each electrical parameter of the converter main switch S_1 at load P_L = 200W.

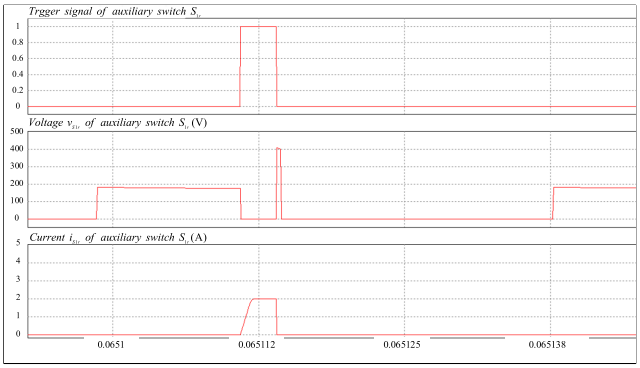

FIGURE 20. Simulated waveforms of each electrical parameter of the converter auxiliary switch S_{1r} at load P_L = 200W.

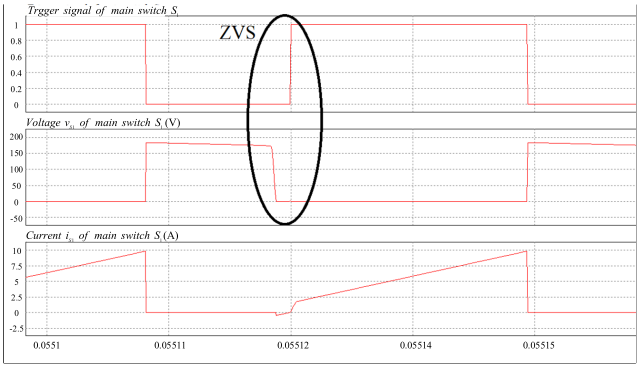

FIGURE 21. Simulated waveforms of each electrical parameter of the converter main switch S_1 at load P_L = 300W.

soft-switching converter to verify the conversion performance of the converter under different load. The converter has been simulated considering the turn ratio $N = 2$, and the simulated specifications are consistent with Table 3. However, the duty cycle will vary according to the load but it must be within 0.65. The lower the input voltage and the heavier load, the higher duty cycle required. Figure 16 shows the simulation results of the output voltage V_H, input voltage V_S, and duty cycle D with the converter working at full load of $P_\text{L} = 300$ W. When the duty cycle was about 0.64, the input voltage of 70 V increased to the output voltage of 400 V. Therefore, the

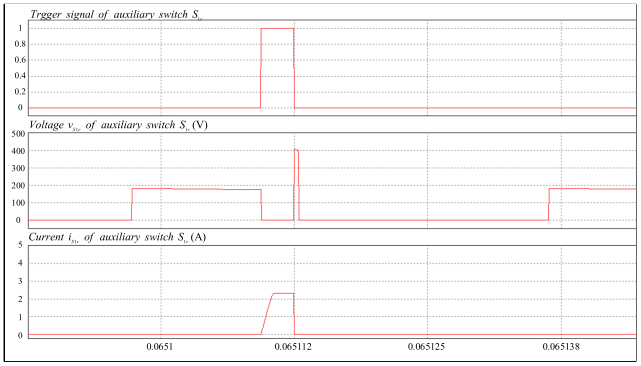

FIGURE 22. Simulated waveforms of each electrical parameter of the converter auxiliary switch S_{1r} at load $P_L = 300W$.

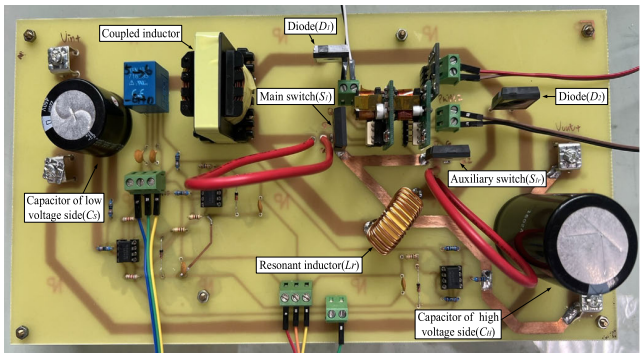

FIGURE 23. Appearance of actual high step-up soft-switching boost converter circuit.

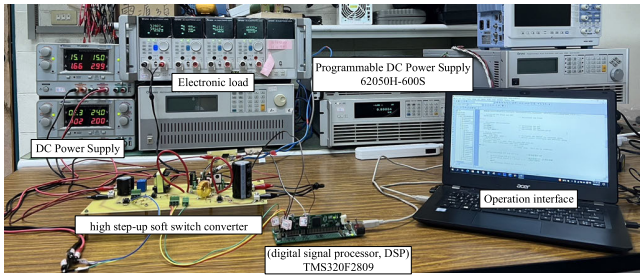

FIGURE 24. Operating environment of actual high step-up soft-switching boost converter circuit.

converter has the characteristic of high step-up ratio. Fig. 17 to Fig. 22 are the switch waveforms of the main switch S_1 and the auxiliary switch S_{1r} of the proposed converter at loadings of $P_L = 100W$, 200W, and 300W, respectively, where the simulated waveforms of each electrical parameter are compliant with the switch waveforms in Fig. 7. Furthermore, it can be seen from the simulated results that the main switch S_1 can all achieve characteristics of zero-voltage switching under different load.

V. TEST RESULTS

After verifying the feasibility of the proposed converter with the PSIM simulated software, use the digital signal processor TMS320F2809 [21] as the control core to conduct the actual

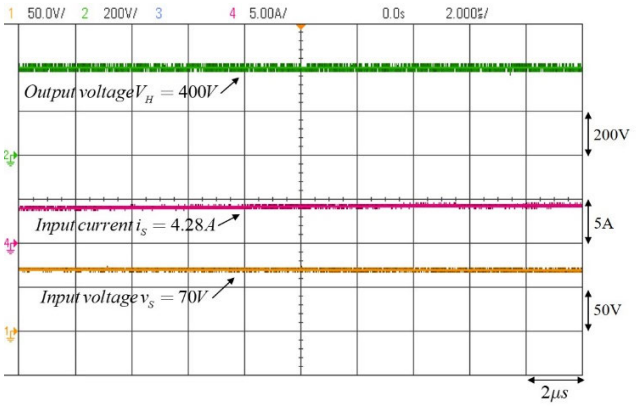

FIGURE 25. Steady state response waveform of the output voltage, input current, and input voltage of converter when operated at load $P_L = 300W$.

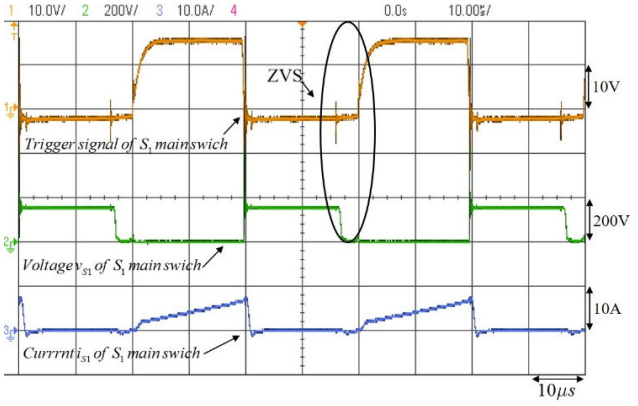

FIGURE 26. Measured waveforms of each electrical parameter of the converter main switch S_1 at load $P_L = 100W$.

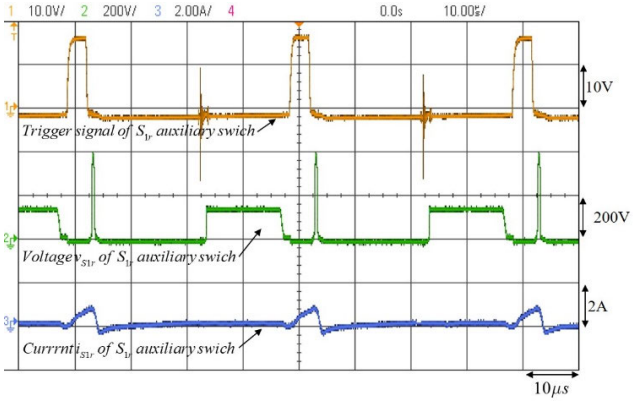

FIGURE 27. Measured waveforms of each electrical parameter of the converter auxiliary switch S_{1r} at load $P_L = 100W$.

testing of the high step-up soft-switching converter; the actual appearance of the whole circuit is as shown in Fig. 23, and the operating environment is shown in Fig. 24. Fig. 25 is the steady state response waveform of the output voltage, input current, and input voltage of the proposed converter when operated at load $P_L = 300W$. It can be observed from Fig. 25 that the output voltage can be controlled at 400V.

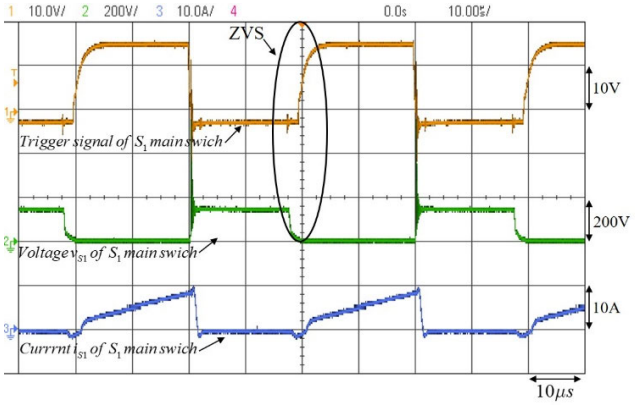

FIGURE 28. Measured waveforms of each electrical parameter of the converter main switch S_1 at load P_L = 200W.

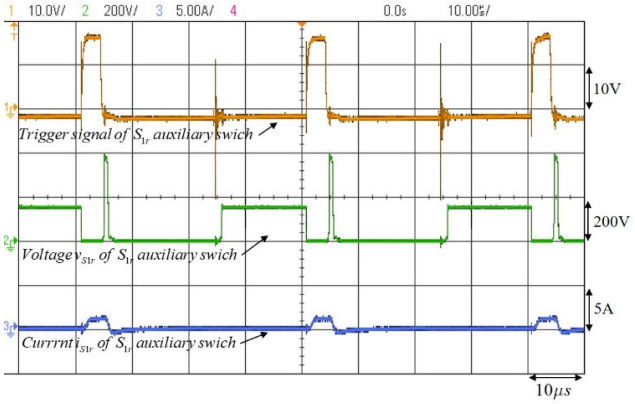

FIGURE 29. Measured waveforms of each electrical parameter of the converter auxiliary switch S_{1r} at load P_L = 200W.

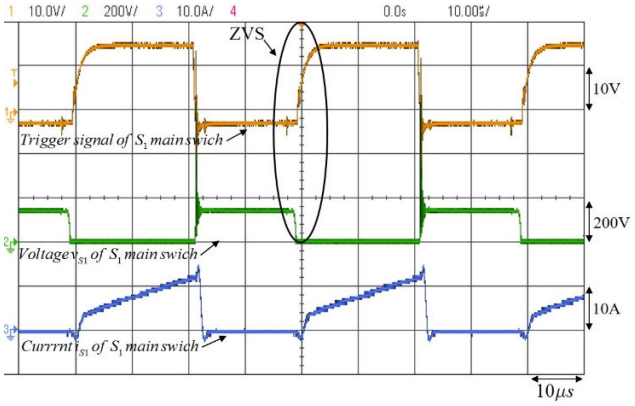

FIGURE 30. Measured waveforms of each electrical parameter of the converter main switch S_1 at load P_L = 300W.

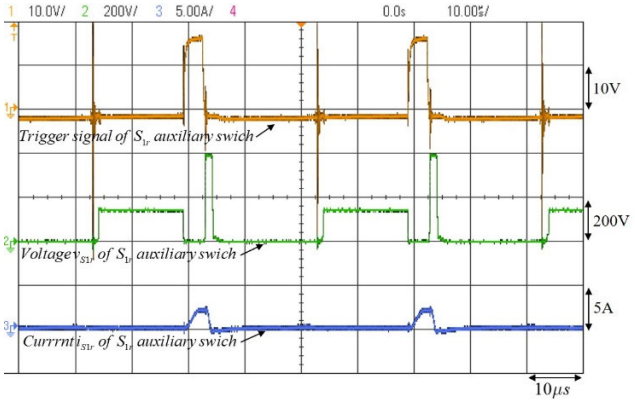

FIGURE 31. Measured waveforms of each electrical parameter of the converter auxiliary switch S_{1r} at load P_L = 300W.

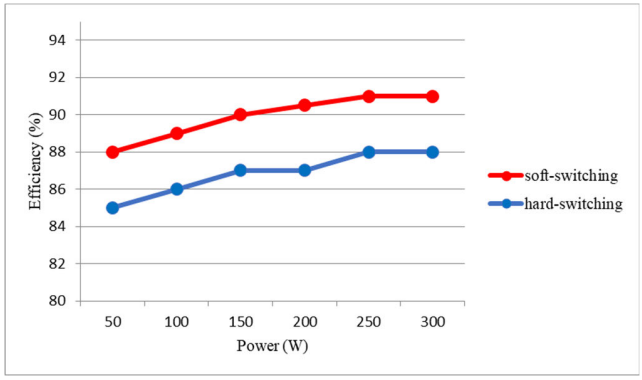

FIGURE 32. Measured efficiency comparison between the proposed soft-switching converter and the traditional hard-switching converter.

Then, Fig. 26 to Fig. 31 are the measured waveforms of the trigger signals, voltage, and current of the main switch S_1 and auxiliary switch S_{1r} when the load of the proposed converter is at P_L = 100W, 200W, and 300W. From the test results, it can be observed that the main switch S_1 can all achieve the characteristics of the zero-voltage switching when the proposed converter is put under different load, and that the measured waveforms and the simulated waveforms of each electrical parameter of the main switch S_1 and auxiliary switch S_{1r} are compliant.

It is proven from the test results that the main switch S_1 of the proposed high step-up soft-switching converter can all achieve soft-switching under load conditions of P_L = 100W, 200W, and 300W, thereby effectively reducing the switching loss of the converter, and increasing the overall efficiency. Fig. 32 is the efficiency comparison result between the proposed high step-up soft-switching converter and the traditional hard-switching high step-up converter under loads from P_L = 50W to P_L = 300W. It is proven in the figure that the efficiency of the proposed soft-switching converter is increased by around 3% under different load conditions when compared with the traditional hard-switching converter.

VI. CONCLUSION

Upon verifying the feasibility of the circuit structure of the high step-up soft-switching converter proposed in this paper with the simulated analysis, and using the TMS320F2809 digital signal processor as the control core to implement the switching control of the converter, it has been proven that the converter can achieve main switch zero-voltage switching

characteristics. The circuit structure has adopted the coupled inductor over the general inductor and utilized the turns ratio of the couple inductor to increase the voltage gain, so that it is able to have a broader input voltage range under high output voltage. Further, since the proposed converter adopted the soft-switching technique, the problem of large switching power loss in hard-switching converter can be improved, thereby improving the overall efficiency of the converter. The proposed converter has advantages of the trigger signal for ease of control, simple circuit structure, and a design with quantifiable component parameter values, and its efficiency is increased by 3% under different load conditions. Its highest conversion efficiency can reach as high as 91%, therefore the proposed converter does indeed have outstanding conversion performance. This converter can be realistically applied to photovoltaic module arrays to undergo maximum power point tracking, thus increasing the power generation efficiency.

REFERENCES

[1] D. Venkatramanan and V. John, "Dynamic modeling and analysis of buck converter based solar PV charge controller for improved MPPT performance," *IEEE Trans. Ind. Appl.*, vol. 55, no. 6, pp. 6234–6246, Nov. 2019.
[2] É. A. Tonolo, J. W. M. Soares, E. F. R. Romaneli, and A. A. Badin, "Current sensorless MPPT with a CCM interleaved boost converter for renewable energy system," *IEEE Trans. Power Electron.*, vol. 37, no. 9, pp. 11296–11304, Sep. 2022.
[3] R. B. Bollipo, S. Mikkili, and P. K. Bonthagorla, "Hybrid, optimal, intelligent and classical PV MPPT techniques: A review," *CSEE J. Power Energy Syst.*, vol. 7, no. 1, pp. 9–33, Jan. 2021.
[4] B. Subudhi and R. Pradhan, "A comparative study on maximum power point tracking techniques for photovoltaic power systems," *IEEE Trans. Sustain. Energy*, vol. 4, no. 1, pp. 89–98, Jan. 2013.
[5] M. Forouzesh, Y. P. Siwakoti, S. A. Gorji, F. Blaabjerg, and B. Lehman, "Step-up DC–DC converters: A comprehensive review of voltage-boosting techniques, topologies, and applications," *IEEE Trans. Power Electron.*, vol. 32, no. 12, pp. 9143–9178, Dec. 2017.
[6] T.-J. Liang, H.-H. Liang, S.-M. Chen, J.-F. Chen, and L.-S. Yang, "Analysis, design, and implementation of a bidirectional double-boost DC–DC converter," *IEEE Trans. Ind. Appl.*, vol. 50, no. 6, pp. 3955–3962, Nov./Dec. 2014.
[7] Y.-C. Hsieh, T.-C. Hsueh, and H.-C. Yen, "An interleaved boost converter with zero-voltage transition," *IEEE Trans. Power Electron.*, vol. 24, no. 4, pp. 973–978, Apr. 2009.
[8] S. Sathyan, H. M. Suryawanshi, M. S. Ballal, and A. B. Shitole, "Soft-switching DC–DC converter for distributed energy sources with high step-up voltage capability," *IEEE Trans. Ind. Electron.*, vol. 62, no. 11, pp. 7039–7050, Nov. 2015.
[9] W. Hassan, J. L. Soon, D. D.-C. Lu, and W. Xiao, "A high conversion ratio and high-efficiency bidirectional DC–DC converter with reduced voltage stress," *IEEE Trans. Power Electron.*, vol. 35, no. 11, pp. 11827–11842, Nov. 2020.
[10] L. He, Z. Zheng, and D. Guo, "High step-up DC–DC converter with active soft-switching and voltage-clamping for renewable energy systems," *IEEE Trans. Power Electron.*, vol. 33, no. 11, pp. 9496–9505, Nov. 2018.
[11] Y. Zheng, B. Brown, W. Xie, S. Li, and K. Smedley, "High step-up DC–DC converter with zero voltage switching and low input current ripple," *IEEE Trans. Power Electron.*, vol. 35, no. 9, pp. 9426–9429, Sep. 2020.
[12] K. H. Chao and C. H. Huang, "Bidirectional DC–DC soft-switching converter for stand-alone photovoltaic power generation systems," *IET Power Electron.*, vol. 7, no. 6, pp. 1557–1565, Jun. 2014.
[13] C.-M. Wang, "Novel zero-voltage-transition PWM DC–DC converters," *IEEE Trans. Ind. Electron.*, vol. 53, no. 1, pp. 254–262, Feb. 2006.
[14] K.-H. Chao and Y.-C. Jheng, "A soft-switching coupled inductor bidirectional DC–DC converter with high conversion ratio," *Int. J. Electron.*, vol. 105, no. 1, pp. 164–190, Jul. 2017.
[15] F. Li and H. Liu, "A cascaded coupled inductor-reverse high step-up converter integrating three-winding coupled inductor and diode–capacitor technique," *IEEE Trans. Ind. Informat.*, vol. 13, no. 3, pp. 1121–1130, Jun. 2017.
[16] S. B. Santra, D. Chatterjee, and Y. P. Siwakoti, "Coupled inductor based soft switched high gain bidirectional DC–DC converter with reduced input current ripple," *IEEE Trans. Ind. Electron.*, vol. 70, no. 2, pp. 1431–1443, Feb. 2023.
[17] S. W. Lee and H. L. Do, "High step-up coupled-inductor cascade boost DC–DC converter with lossless passive snubber," *IEEE Trans. Ind. Electron.*, vol. 65, no. 10, pp. 7753–7761, Oct. 2018.
[18] F. Yang, C. Li, Y. Cao, and K. Yao, "Two-phase interleaved boost PFC converter with coupled inductor under single-phase operation," *IEEE Trans. Power Electron.*, vol. 35, no. 1, pp. 169–184, Jan. 2020.
[19] B. L. Narasimharaju, S. P. Dubey, and S. P. Singh, "Coupled inductor bidirectional DC–DC converter for improved performance," in *Proc. Int. Conf. Ind. Electron., Control Robot.*, Rourkela, India, Dec. 2010, pp. 27–29.
[20] (Jan. 2021). Powersim. [Online]. Available: https://powersimtech.com/wp-content/uploads/2021/01/PSIM-User-Manual.pdf
[21] Texas Instruments. (Oct. 2003). *TMS320F2809 Data Manual*. [Online]. Available: https://www.ti.com/lit/ds/symlink/tms320f2809.pdf?ts=1594465026502&ref_url=https%253A%252F%252Fwww.ti.com%252Fproduct%252FTMS320F2809

KUEI-HSIANG CHAO (Member, IEEE) received the B.S. degree in electrical engineering from the National Taiwan University of Science and Technology, Taipei, Taiwan, in 1988, and the M.S. and Ph.D. degrees in electrical engineering from National Tsing Hua University, Hsinchu, Taiwan, in 1990 and 2000, respectively. He is currently a lifetime Distinguished Professor with the National Chin-Yi University of Technology, Taichung, Taiwan. His research interests include computer-based control systems, the applications of control theory, renewable energy, and power electronics. He is a Life Member of the Solar Energy and New Energy Association.

YING-PIAO KUO received the B.S. degree in electrical engineering from the National Taiwan University of Science and Technology, Taipei, Taiwan, in 1985, the M.S. degree in electrical engineering from National Taiwan University, in 1989, and the Ph.D. degree from the National Taiwan University of Science and Technology, in 2011. In 1989, he joined the National Chin-Yi University of Technology, Taichung, Taiwan, where he is currently an Associate Professor with the Department of Electrical Engineering. His current research interests include the design of switching-mode power supplies, the speed estimation of ac motor drives, partial discharge, and power system stability.

HONG-HAN CHEN was born in Taipei, Taiwan, in 1999. He received the degree in electrical engineering from the National Chin-Yi University of Technology, Taichung, Taiwan, in 2021, where he is currently pursuing the Graduate degree with the Electrical Engineering Department. His research interests include renewable energy, power electronics, and maximum power point tracking for photovoltaic module arrays.